Research Article

Emergency Separation Simulation and Damage Prediction of an Airliner under Wheel-Up Landing Condition

Pengfei Zhang [ID],[1,2] **Hong Nie** [ID],[1] **Jianfei Wu**,[1,2] **and Muqi Yu** [ID][1]

[1]*College of Aerospace Engineering, Nanjing University of Aeronautics and Astronautics, Nanjing 210016, China*
[2]*Structure and Stress Department, Shanghai Aircraft Design and Research Institute, Shanghai 201206, China*

Correspondence should be addressed to Pengfei Zhang; zhangpengfei@comac.cc

To predict the damage to and response of aircraft structures during wheel-up crash landing, numerical simulations were performed using a constitutive and damage model for ductile metallic materials developed in the ABAQUS/Explicit environment. The model of an entire aircraft and detailed submodels were established. The Johnson–Cook and Gurson material constitutive models were validated by conducting Hopkinson's bar test. A drop hammer test and a static test of the fuse pins were performed to determine and verify the response and strength of the structure. The experimental and analytical results indicate that the stain rate and damage parameters significantly influence the emergency separation load, fuse pin strength, and separation sequence. The analysis results were compared with the test results, and a close agreement was found in terms of the maximum load and deformation.

1. Introduction

The protection of fuel tanks and cabins during takeoff and emergency landing of civil aircraft is a critical topic in aircraft design. Wing-mounted engine has emerged as the primary configuration of civil aircraft. In these aircraft, the distance between the nacelle and the ground is small, especially in the wheel-up landing condition. Although most emergency landing events are relatively controllable, the nacelle inevitably comes into contact with the ground. Therefore, the wing and fuel tank structures should be designed such that they are not damaged during primary and secondary impacts to the airframe. Civil aviation regulation Part 25 requires an aircraft to sink at a speed of at least 1.52 m/s (5 fps) and in a maneuverable state to avoid damage to the fuel tank when it crashes on the ground with the maximum landing weight. Moreover, the landing gear should be fully retracted, and any other combination of landing gear legs should not be extended. It needs to be combined with a slip angle of up to 20° [1]. In addition, protection of the fuel tank structure and cabin occupants should be considered in extreme cases, where loads and

forces exceed those associated with the abovementioned design conditions. In general, fuse pins are mounted between the pylon and the wing structure. In a crash event where the impact load generated by the crash is greater than the strength of the fuse pins, for instance, when the aircraft sinking speed exceeds the threshold speed, the fuse pins fail, and the nacelle breaks away from the wing structure.

To meet the requirements of regulation [1], it is necessary to obtain accurate dynamic loads and ensure that the engine and the nacelle break away from the wing. For configurations where the nacelle may come into contact with the ground, nacelle separation designs are widely used to protect the wing and the fuel tank structure. Moreover, it must be ensured that the fuel tank structure near the engine and nacelle will not fail during a crash and separation. Many researchers have extensively studied emergency separation designs. G. Chen et al. developed a method of modeling and simulation for coupled crash mechanics and biomechanics of aircraft structures and passengers [2]. Jin et al. studied the method of crash simulation of fuselage section in the rebound process and the secondary-impact process [3]. Bronstein et al. developed a method to assess the dynamic

effects on aircraft design loads [4]. Wang et al. developed a method for determining horizontal impact load [5]. Li developed an analytical method to compute the crash load during a wheel-up landing event [6]. Zhang developed a numerical simulation method to analyze the fuselage section [7]. Liu et al. developed a method to conduct crash tests of the fuselage section and cabin facilities [8]. Iqbal et al. developed a numerical simulation method of aircraft crash on nuclear containment structure [9]. Owing to the increasing complexity of essential systems such as landing gear, the associated regulations have become stricter. Fuse pins are installed between the nacelle and the wing for transferring loads from the engine. A fuse pin fails when the structure is overloaded in an emergency landing event, and as a result, the engine and nacelle break away from the aircraft. This process represents a highly nonlinear dynamic problem that is influenced by multiple factors such as sinking speed, approach speed, and pitch angle. Traditional linear finite element (FE) methods, engineering algorithms, and experimental methods cannot be used to analyze the stress, strain, strength, and fracture of the aircraft structure in a crash event.

In 1978, Morjarai used the FE method to analyze elastoplastic coupling of transient thermal stress in a small deformation range [10]. Subsequently, the elastoplastic finite element method that combines temperature field functions and displacement field functions has been widely used to solve thermomechanical coupling problems such as metal forging, extrusion, and steel rolling [11–13]. In addition, the algorithm for coupling plastic FEs with temperature field FEs has been widely used. In 1993, Ponier used Euler's method to establish a thermoplastic coupling FE model based on constitutive relationship hardening and strain hardening [14]. In 1995, Lin studied the deformation of aluminum strips under different temperature cooling methods by using the large deformation FE theory of Lagrangian elements [11]. In 1998, Rodrigues analyzed changes in the plane strain of a rolled steel plate by using a combination of the boundary element method (BEM) and the FE method [15]. Bragov et al. developed a method of experimental and numerical analysis of high strain rate response of Ti-6Al-4 V titanium alloy [16]. Wu and Haijun studied a coupled FEM/BEM method with linear continuous elements for solving acoustic-structural interaction problems [17]. In 1999, Dyja and Korczak analyzed the deformation of a plate and the microstructural changes in the plate material during plate rolling [18]. In 2006 Boogaard established a material constitutive equation based on the stress-strain curve of a material at different temperatures and studied the effects of temperature change, strain rate, and flow stress on the mechanical properties of the material by conducting a FE thermomechanical coupling analysis. In 2012, Zhou directly input the stress-strain curve as a thermomechanical coupled FE material model and simulated the mechanical behavior of materials at different temperatures [19]. Malcher studied the constitutive parameters of ductile metallic materials [14]. Tanaka et al. developed a mechanical experimental method for double shear fitting [20].

In light of these problems, the thermolytic coupling FE method can be used to simulate the structure fracture process and quantitatively analyze the failure modes of various fuse pin configurations. We herein predict fuse pin damage and strength in the wheel-up landing condition by using the nonlinear explicit solver ABAQUS/Explicit. In addition, we propose a method for FE analysis, contact definition, and load calculation, as well as a material constitutive and damage model, for emergency separation analysis. The influence of the above factors on structural strength and emergency separation design are investigated.

2. Numerical Simulation

The proposed simulation model for emergency separation analysis covers the following aircraft parts: fuselage, wing, nacelle, and fuse pins. Among them, the fuselage and wing mainly provide stiffness, and the nacelle is modeled to simulate contact with the ground. The strength and dynamic characteristics of the fuse pins are critical factors in the emergency separation design. It requires not only a definite lower limit of strength but also an upper limit of strength. The simulation model is composed of various structures and materials. In this study, the simulation and experiments are carried out in the material constitutive and damage modes to study the separation process and response history. In addition, the responses of the tires and the landing gear during landing directly affect the analysis results. For this reason, the impact properties of the landing gear and the tires are studied as well. The separation design of a single-channel narrow-body aircraft is investigated using the ABAQUS/Explicit solver.

2.1. Finite Element Model. The frame-beam-panel combined structure is typically used in modern civilian aircraft because it can not only meet the requirements of strength and stiffness but also reduce weight. The materials are mainly 2000 and 7000 series aluminum alloys. In case of the nacelle and pylon, Ti-6Al-4V and high-temperature alloy stainless steel are partially used to fulfill fireproofing requirements. In the simulation, to simulate the load and impact in the event of an aircraft crash, it is necessary to analyze the entire model and simulate and analyze the fracture and failure of local structures. For the entire aircraft model, to improve the calculation efficiency and ensure calculation accuracy, different FE modeling strategies are adopted for each aircraft region. For the fuselage area (yellow area), which is not subjected to impact loads, two-dimensional surface elements and one-dimensional elements with a coarse mesh are used in the simulation. For the part of the body structure that is subjected to impact loads, a two-dimensional (2D) plate element S4R (blue area) is used in the simulation. For the areas connected to the emergency disconnection device, including wing joint, hanger, and nacelle, refined body elements are used (see Figure 1). B31 beam elements are used to simulate the beam and stiffener; S4R shell elements are used to simulate the panel and skin; and two-force bar elements are used to simulate the interface connecting the rod
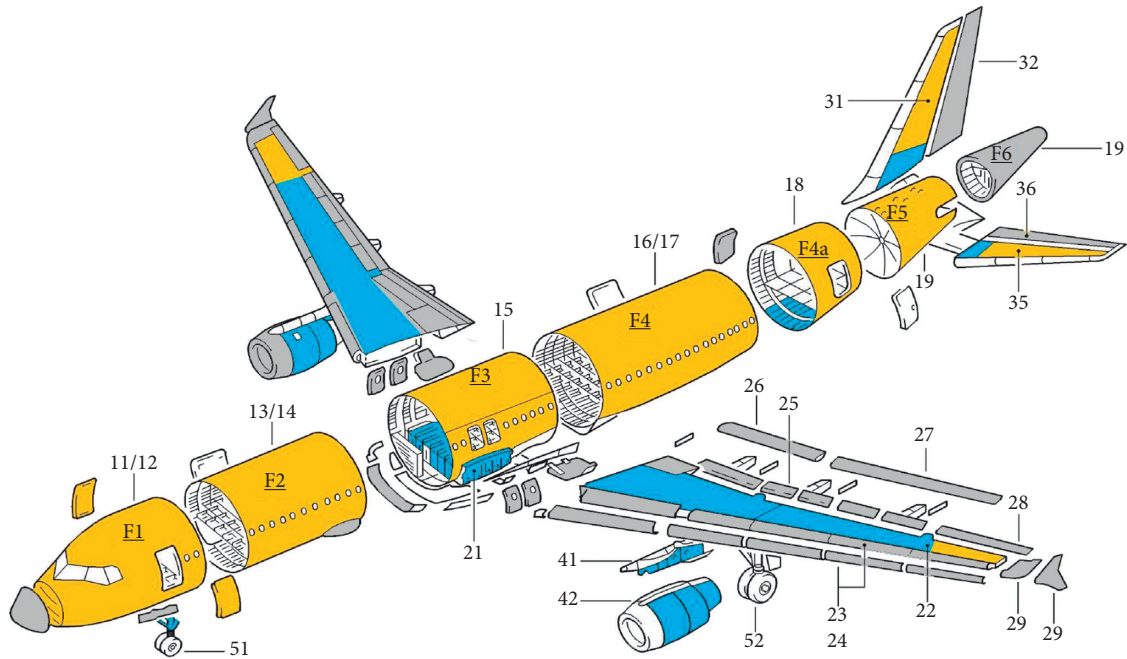
Figure 1: Structure of a typical large civilian aircraft.

structure. The joints, pins, and structures are simulated using C3D8R 3D volume elements in the structure docking position. Moreover, C3D8R elements are used to simulate the emergency disconnection structure. The engine is simulated using high-stiffness beam elements; mass and inertia characteristics are simulated using lumped mass elements; and the nacelle structure is simulated using S4R panel elements and C3D8R 3D volume elements. By setting the basic size of the finite element mesh to 5 mm, we obtain slightly different grid densities for different parts of the structure. The entire model contains 293,450 nodes, 303,057 units, 32 MPCs, and material parameters.

The pylon structure is composed of titanium, aluminum, and steel. Young's moduli and Poisson ratios of the materials are summarized in Table 1. Throughout the model, beam elements are used to simulate bolts and pins, and spring elements are used to simulate the connections between the pylon and the wings. The elements used to simulate pins are assigned a large bending stiffness to simulate the bending stiffness of bolt (generally $> 10^7 \, mm^4$). Moreover, shear stiffness is used to simulate the transfer of attachment loads. Shell elements are suitable for modeling most areas of the wing, pylon, and cabin structures. Because of the thickness of attachments, 3D elements are used. Moreover, connections between 2D and 3D elements are realized by sharing multilayer nodes that can constrain only translational freedom. To simulate the bending stiffness of the structure correctly, the coupling constraints are simulated using rigid 2D and 3D elements. The wheel-up landing condition involves not only the scenario in which both main gears are retracted but also the scenario in which any one of the landing gears is retracted. This process relies on the landing gears to absorb energy during landing. The landing gear is composed of a gear structure, shock absorbers, and tires. The performance of the shock absorber and tires needs to be simulated in the model to accurately compute dynamic loads and damage to the structure (see Figure 2).

2.2. Fuse Pin Model. Modeling of the fuse pins is the key task in the simulation of emergency separation. In this study, the fuse pin structure is modeled using refined hexahedral reduction integral elements C3D8T (see Figure 3). The basic meshing size is 0.5 mm, and the meshing size for the fitting lugs is 3.5 mm. Contact can be simulated in terms of interactions between the structures, and it is necessary to ensure that the components do not penetrate without interaction and influence. Three types of contact situations need to be considered: contact between the fuse pins and fittings; mutual contact due to deformation or movement of the joint itself, such as contact between the lugs and other parts; and contact between the pylon and wing fittings. For contact between the fuse pins and the hole wall, which involves calculating subsequent contact between the inner parts after failure of the outer elements of the fuse pin, nodes-to-surface contact is assigned. The surface of the joint with refined meshes is set as the master surface, and the fuse pin nodes are slave nodes. For the contact due to deformation between fitting lugs and contact between the bottom of the lugs and the pylon, surface-to-surface contact is adopted, and the contact area between the surfaces is automatically determined. The contact considers limited slip, and the tangential friction coefficient is set to 0.15 (see Figure 4).

3. Materials

3.1. Material Constitution. In wheel retraction and crash analyses, the focus is on the material parameters of the product structures that may be damaged during a crash.

TABLE 1: Material properties.

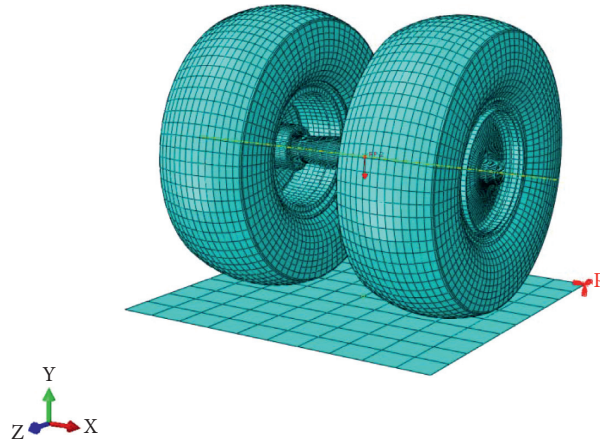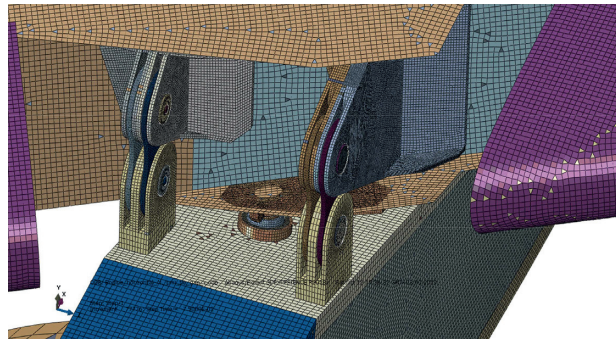| Material	Young's modulus (MPa)	Poisson ratio	σ_b (MPa)	σ_y (MPa)
Titanium (Ti-6Al-4 V)	110000	0.31	930	827
Aluminum (7050)	71000	0.33	544	489
Stainless steel (15-5PH)	196365	0.27	1089	1000

FIGURE 2: Model of landing gear tires.

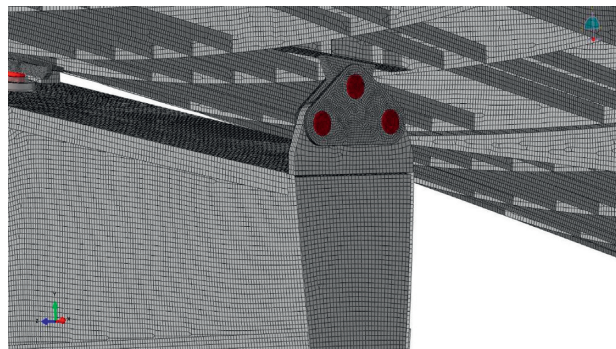FIGURE 3: FE model of separation structure.

FIGURE 4: FE model of separation structure.

Titanium alloy Ti-6Al-4V and 2000 series and 7000 series aluminum alloys are widely used in aircraft structures. The structure and damage models are created using the progressive material damage model available in ABAQUS. The behavior of this material is described using the modified GURSON model, TVERGAARD factor, and a rate-dependent multiplier [6]. In this model, the plasticity criterion is implemented as a GURSON potential function.

Fiber-reinforced composites are widely used in aircraft wing structures, and therefore, the constitutive parameters

of wing structures are different from those of metallic structures. According to the stress and failure modes of the wing structure and the engine hanging joint, by referring to Hashin's theory [21, 22], four different failure initiation mechanisms are considered for the composite material

constitutive parameters in the wheel retraction crash analysis: fiber tension, fiber compression, matrix tension, and matrix compression. The general form of the starting condition is as follows:

$$\text{Fiber tension}\left(\widehat{\sigma}_{11} \geq 0\right): F_f^t = \left(\frac{\widehat{\sigma}_{11}}{X^T}\right)^2 + \alpha\left(\frac{\widehat{\tau}_{12}}{S^L}\right)^2,$$

$$\text{Fiber Compression}\left(\widehat{\sigma}_{11} < 0\right): F_f^c = \left(\frac{\widehat{\sigma}_{11}}{X^C}\right)^2,$$

$$\text{Matrix tension}\left(\widehat{\sigma}_{22} \geq 0\right): F_m^t = \left(\frac{\widehat{\sigma}_{22}}{Y^T}\right)^2 + \left(\frac{\widehat{\tau}_{12}}{S^L}\right)^2,$$

$$\text{Matrix Compression}\left(\widehat{\sigma}_{22} < 0\right): F_m^c = \left(\frac{\widehat{\sigma}_{22}}{2S^T}\right)^2 + \left[\left(\frac{Y^C}{2S^T}\right)^2 - 1\right]\frac{\widehat{\sigma}_{22}}{Y^C} + \left(\frac{\widehat{\tau}_{12}}{S^L}\right)^2 0.$$

(1)

In the formula, X^T represents longitudinal tensile strength, X^C represents longitudinal compressive strength, Y^T represents transverse tensile strength, Y^C denotes transverse compressive strength, S^L denotes longitudinal shear strength, S^T denotes transverse shear strength, and α denotes the initial criterion for determining the effect of shear stress on fiber stretching. The aforementioned starting criteria can be specifically used to obtain the model proposed in Hashin and Rotem [10] by setting or to obtain the model proposed in Hashin (1980) by setting.

3.2. Damage Model.
According to the Hooputra theoretical formula, in ABAQUS/Explicit, the damage model can be defined simultaneously with the elastoplastic constitutive models of Mises, Johnson–Cook, Hill, and Drucker-Prager to simulate the material damage process. The simulation method assumes that each attenuation in stiffness due to effective failure mechanism can be modeled using a scalar damage variable, which represents a series of effective failure mechanisms. The stress tensor associated with the process of material damage is expressed using the following scalar damage equation:

$$\sigma_d = (1 - D)\overline{\sigma}_i. \tag{2}$$

In this equation, D denotes the global damage variable, which represents the stress tensor in the case of no damage. When the value of D is 1, the material loses its strength completely. Generally, when any integrated location in the structure loses its ability to transfer load, the associated elements are removed from the model. It explains the characteristics of the stress-strain curve and the mechanical properties of the metallic material after damage (see Figure 5). In the case of isotopically hardened elastoplastic materials, damage is manifested as a reduction in flow stress and plasticity. The solid line denotes the stress-strain

behavior of the material after damage, and the dashed line represents the absence of damage.

σ_{y0} and ε_0^{-pl}, respectively, refer to the yield stress and the equivalent plastic strain when material damage is initiated, ε_f^{-pl} denotes the equivalent plastic strain at the point of complete material failure (that is, the global damage variable $D = 1$) (see Figure 6). The value of ε_f^{-pl} at failure depends on the length of the element. The specific parameters must be adjusted according to the mesh density. The law of damage evolution of metallic materials is defined considering the equivalent plastic displacement.

3.3. Material Testing.
The Hopkinson test is conducted to determine the dynamic constitutive material model. In this study, the Hopkinson test was performed using a cylindrical 15-5PH stainless steel sample (see Figures 7 and 8). The tested strain rates were $640\,\mathrm{s}^{-1}$, $1045\,\mathrm{s}^{-1}$, $1378\,\mathrm{s}^{-1}$, and $2075\,\mathrm{s}^{-1}$. The constitutive model was fitted to the measured stress-strain curve, and the constitutive relationship of 15-5PH stainless steel was established.

The flow stress behavior of 15-5PH stainless steel was studied by conducting a split Hopkinson pressure bar (SHPB) compression experiment. The true stress-strain curves of compression deformation of 15-5PH stainless steel at the strain rates of $640\,\mathrm{s}^{-1}$, $1045\,\mathrm{s}^{-1}$, $1378\,\mathrm{s}^{-1}$, and $2075\,\mathrm{s}^{-1}$ are presented in Figure 9. As the strain rate increases, the yield stress of the material increases significantly, indicating that the material is strain rate-sensitive. In addition, the higher the strain rate, the larger the area under the flow stress-strain curve; that is, as the strain rate increases, a greater amount of energy is required to ensure that the curve reaches a specific strain.

The Johnson–Cook constitutive model is a typical macroscopic phenomenological constitutive model. It has good predictive ability over wide ranges of temperatures and strain rates. Therefore, it has been widely used in metal
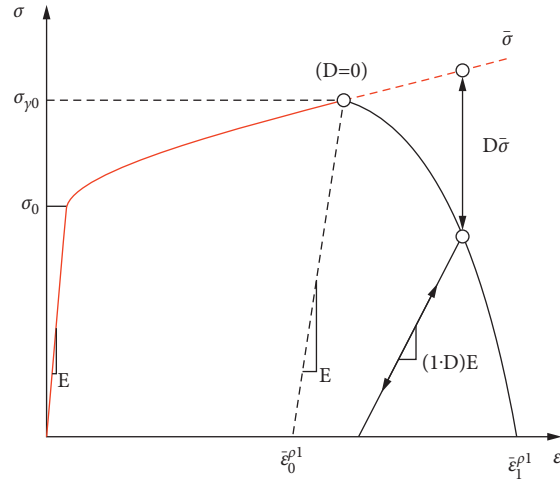
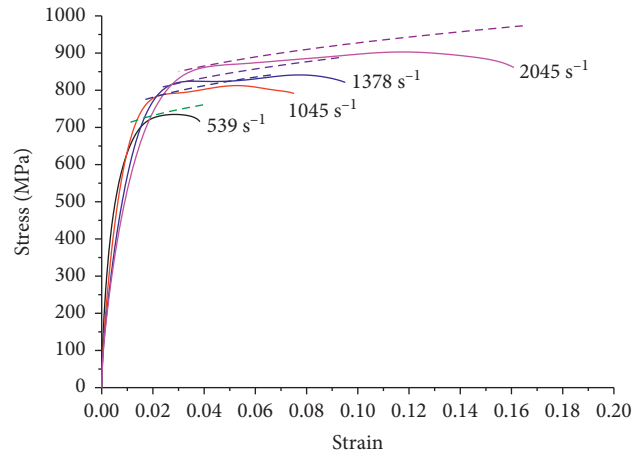Figure 5: Stress-strain relationship of metallic material.

Figure 6: Comparison of Johnson–Cook model and experimental curve under different strain rates.

Figure 7: Hopkinson bar impact test system.

deformation research. Johnson–Cook hardening is a type of isotropic hardening. Considering that the SHPB experiment is conducted at room temperature to obtain the true stress-strain curve at a fixed strain rate, the experimental temperature of the 15-5PH stainless steel material was set to be equal to the reference temperature of the material. Its static stress expression is as follows:

$$\sigma = \left(A + B\varepsilon_p^n\right)\left(1 + C \ln \frac{\dot{\varepsilon}_p}{\dot{\varepsilon}_r}\right). \tag{3}$$

In the above formula, A is the yield strength at the reference strain rate, MPa; B is the strain hardening coefficient, MPa; C is strain rate hardening coefficient; n is strain hardening index; ε_p is equivalent plastic strain; $\dot{\varepsilon}_p$ is equivalent plastic strain rate, s-1; and $\dot{\varepsilon}_r$ is the reference plastic strain rate, s-1.

The constant values associated with the rheological behavior of 15-5PH stainless steel predicted using the Johnson–Cook constitutive model are listed in Table 2. By using this equation, the predicted flow stress values of 15-5pH
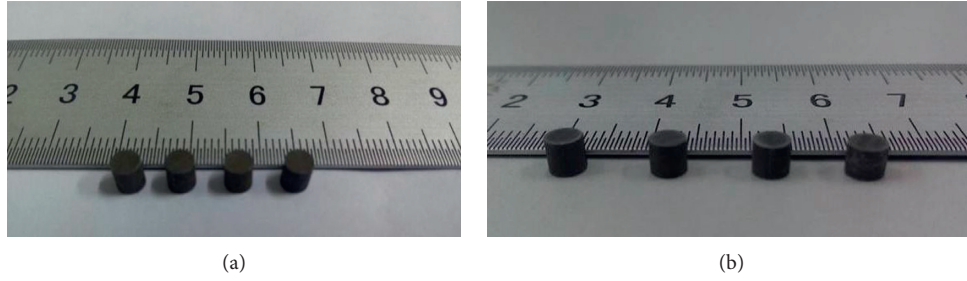
(a)

(b)

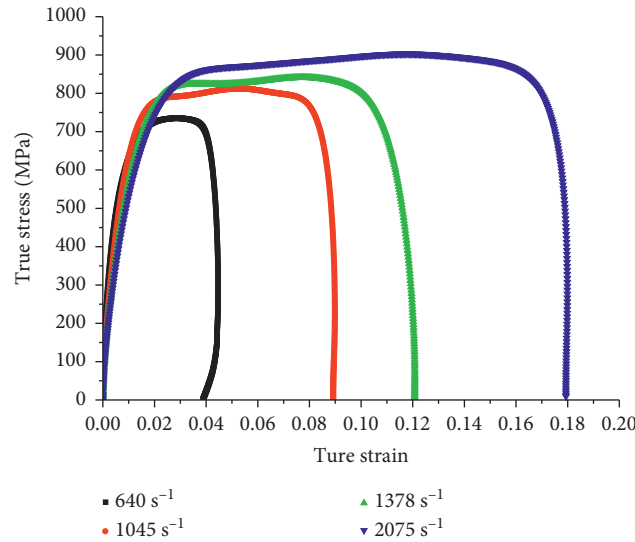Figure 8: Hopkinson test samples. (a) Before test. (b) After test.

Figure 9: Real stress-strain relationship of 15-5PH stainless steel at different strain rates.

Table 2: Calculated Johnson–Cook model parameters for 15-5PH.

Parameters	A (MPa)	B (MPa)	C	n
Value	650	455	0.101	0.4372

stainless steel under four strain rates with different strain values can be computed. Figure 6 presents a comparison of the experimental values and predicted values under four strain rates.

$$\sigma = \left(650 + 455\varepsilon_p^{0.4372}\right)\left(1 + 0.101 \times \ln\frac{\dot{\varepsilon}_p}{\dot{\varepsilon}_r}\right). \qquad (4)$$

The Johnson–Cook constitutive model can be used to describe the rheological behavior of a conforming material over the entire range of plastic strain and different strain rates. In the deformation process, the curve of predicted values coincides with the curve of experimental values in the range of yield strength and plastic deformation. Strain hardening occurs in high strain rate stage. Therefore, the Johnson–Cook constitutive model can well explain the work hardening behavior of 15-5PH stainless steel.

4. Fuse Pin Impact Test

We conducted a drop hammer impact test to determine changes in the strength of the emergency fuse pins and attachments under different levels of impact energy in the wheel-up landing condition, as well as to obtain the impact energy and strength curves. The impact velocity should be greater than 1.524 m/s (5 ft/s), as specified in FAR 27.721(b) [1], and the impact energy was preliminarily estimated by conducting a numerical simulation. The test system was composed of test bench and the drop hammer system (see Figure 10). The test bench is composed of a loading wall, slide, cylindrical sliding track, and joints, and its main structural material was Q235 steel. The height of the test bench and the size of the fixture were determined considering the impact velocity and impact energy requirements during the test. The external dimensions of the test bench
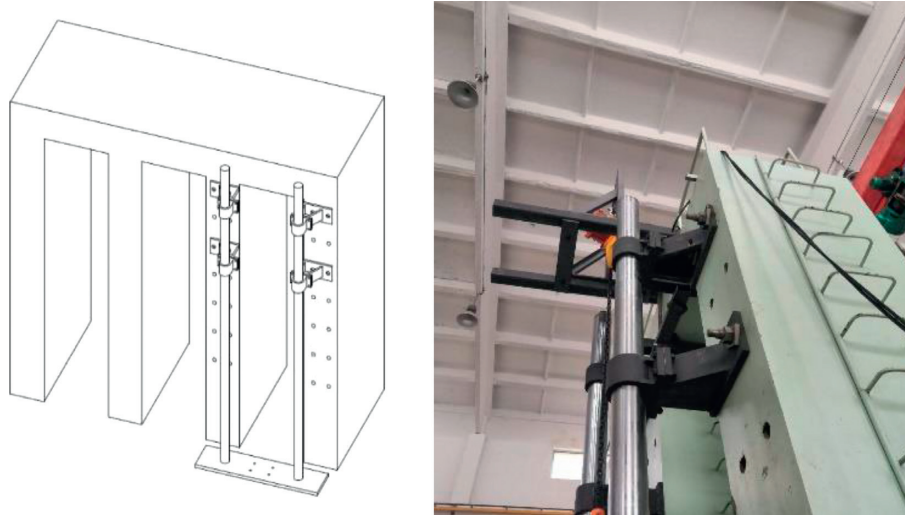
Figure 10: Drop hammer impact testing system.

were 2150 mm × 2790 mm × 5010 mm (length × width × height), and the diameter of the two-cylinder slides was 140 mm. Through two sliding structures, wall and bottom plate, the test setup is formed. At the bottom of the test system, a thick steel plate was used as a support. Considering the impact test load, the supporting bottom beam should be able to withstand a load exceeding 200 tons without undergoing plastic deformation. The thickness of the bottom plate wall was designed as 50 mm.

To study the relationship between the loading rate and fuse pin strength, it is necessary to simulate different impact rates by adjusting the drop height. Through variable parameter analysis, we studied the test impact speed of the emergency fuse pins in a scenario where the gears were retracted and the sinking speed of the wheel was 1.524 m/s (5 ft/s), 2.438 m/s (8 ft/s), 4.572 m/s (15 ft/s), 7.62 m/s (25 ft/s), 10.668 m/s (35 ft/s), and 15.24 m/s (50 ft/s). The maximum lifting height of the hanging basket can reach 3050 mm, which can fulfill the needs of our experiment. A physical diagram of the drop hammer test system is shown in Figure 10.

The simulation results of the fuse pin were compared with the experiment result at the condition that the sinking speed is 2.438 m/s (8 ft/s). The results show that the deformation is in good agreement with the experimental deformation (see Figure 11). From the comparison of stress cut view, the damage shape is similar. For the fuse pin's failure load, the test result is 190 KN when the simulation result is 187 kN. The deviation between simulation and experiment is about 3%.

5. Simulation

5.1. Fuse Pin Simulation. In a numerical simulation of emergency separation, the influence of model discretization and material constitutive and fracture parameters must be considered. Research and analysis of the mesh size of the fuse pins and determination of its relationship with strength capacity are the first step in developing analysis model. The

mesh size is directly related to the degree of deviation of the analysis result from the real situation. In the FE model, the mesh size was gradually reduced from 3.5 mm in steps of 0.1 mm to determine the relationship between mesh size and strength. Figure 12 shows the maximum shear strength of the fuse pins as the mesh size changes. As the mesh size decreases, the shear strength gradually increases and then stabilizes. For mesh sizes smaller than 0.6 mm, it gradually converges. The mesh size of 0.5 mm was used in our analysis (see Figure 12).

The eight-node hexahedral linear reduction integral element C3D8R was used in the simulation, and the mesh size of the bushing and fittings was 2.5 mm (see Figure 13). The structural material of the lugs was titanium alloy, surface-to-surface contact was used in the numerical simulation model, and the friction coefficient was set to 0.15. The connection between the nut and the fuse pins was set as a binding constraint; that is, relative movement between them was restricted. The underside of the lower ear was fixedly supported. A uniform tensile load was applied to the upper surface of the side ear, and this load increased linearly with time.

The damage model used for the fuse pins is a critical aspect of this simulation. Here, we used the shear damage model in ABAQUS to define the material damage relationship, including three parameters: fracture strain, which is characterized by the uniform elongation of the tensile test curve, and 15-5PH stainless steel has a uniform elongation rate of 0.141; shear strain rate; displacement at failure in a suboption of the model, which was determined by conducting a material experiment involving the fuse pin material. The failure displacement measured in this test was 0.95. Before numerical simulation, the damage model of the standard material components was verified. A test piece made of 15-5PH stainless steel conforming dimensionally to the ASTM B769 standard material sample was used herein; an FE model of this sample was developed in ABAQUS by using C3D8R elements, and the mesh size was 0.3 mm. A comparison of the analysis and the test results revealed that
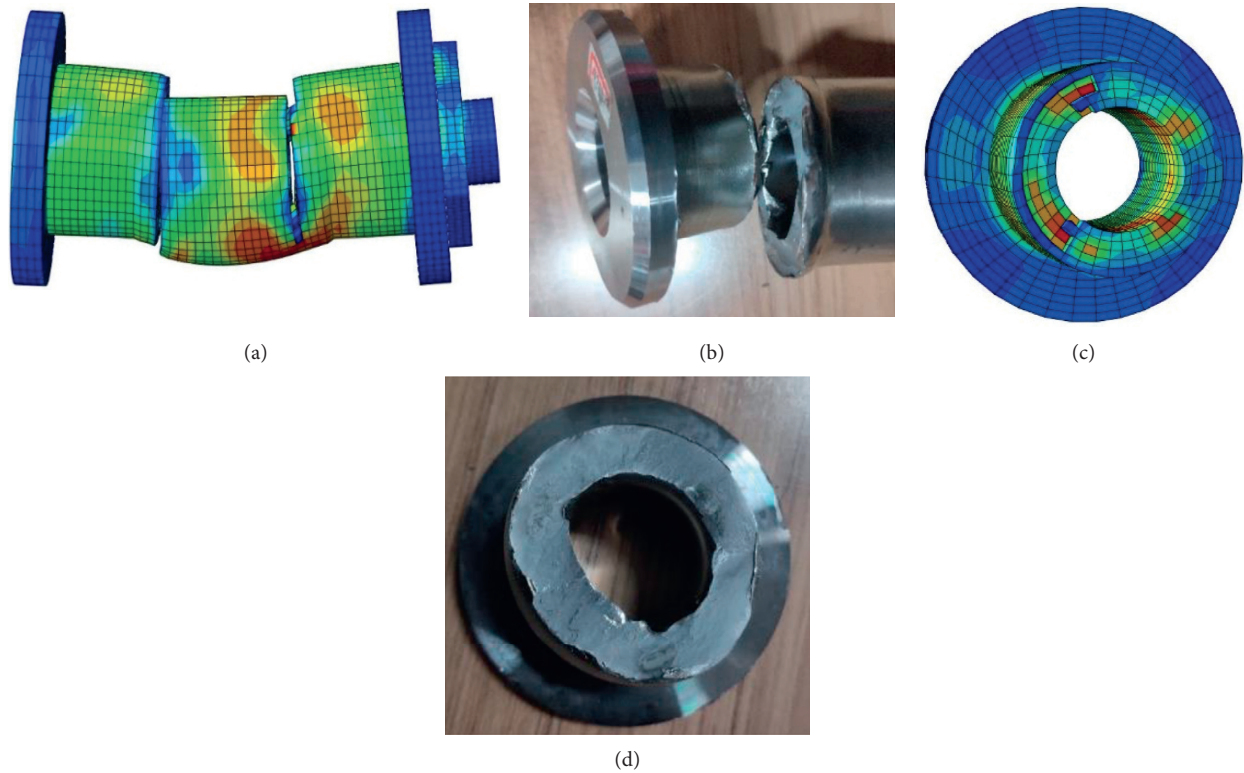
(a)

(b)

(c)

(d)

FIGURE 11: Comparison of test and simulation result. (a) Simulation result of fuse pin. (b) Test results of fuse pin. (c) Cut view of simulation result of fuse pin. (d) Cut view of fuse pin after test.
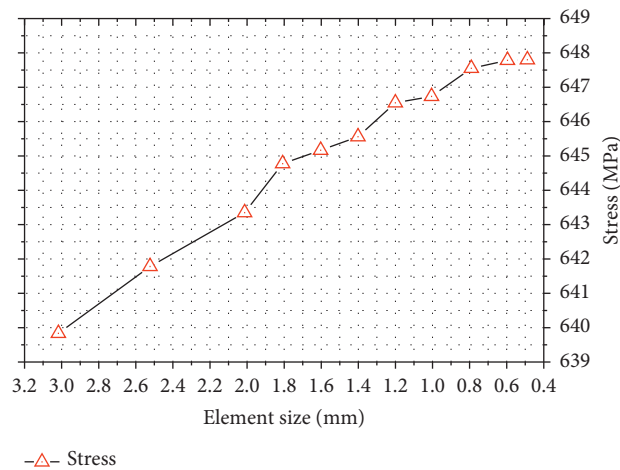

FIGURE 12: Relationship between mesh size and shear strength.

the failure time of the sample (moment of maximum shear strength) was 0.8 s (see Figure 14). The maximum shear strength was 652.7 MPa.

Based on the above results, the simulation model of the separation fuse pin was analyzed and verified, and the model including the lugs, fuse pins, and bushings was established. The structural form of the model was consistent with the configuration of aircraft emergency fuse pins. In the analysis, a full constraint was imposed on the bottom surface of the lower connector, and a binding constraint was imposed on relative movement between the nut and the fuse pin. A uniformly distributed tensile stress was applied to the upper surface of the upper fitting. The hollow uniform cross section shear fuse pin had an inner diameter of 16.95 mm and outer diameter of 42 mm. The theoretically calculated maximum shear stress of the fuse pin before the specimen was cut was 651.7 MPa, and the breaking load was 1450.6 KN. Upon failure of the pin structure, the maximum displacement of the lower fitting was 7.9 mm (see Figures 15–18).

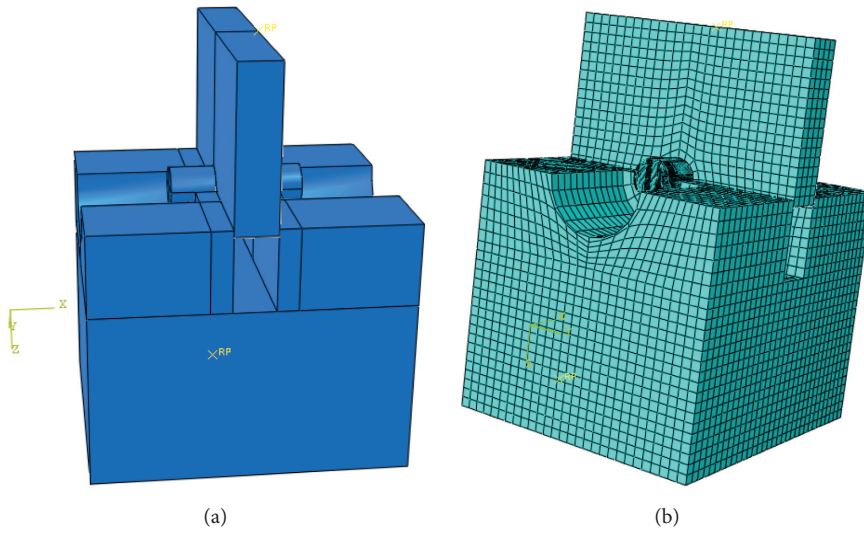(a)   (b)

FIGURE 13: Geometry and simulation model of material shear test. (a) Material test sample and fixture geometry. (b) Material test sample and fixture FE model.

(a)   (b)
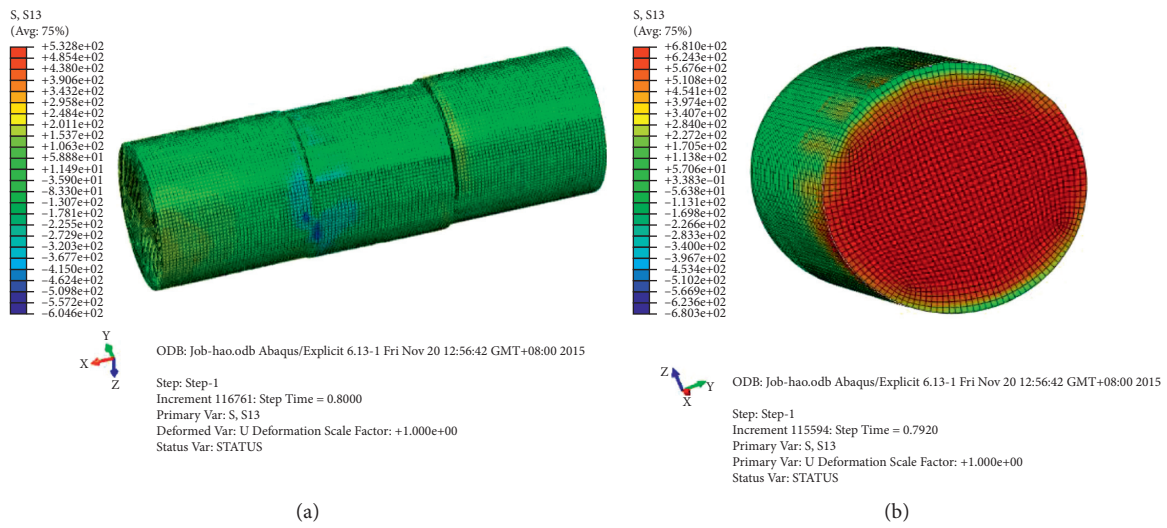
FIGURE 14: Material sample test, and stress contour at time of fracture. (a) Material sample contour. (b) Material sample cut contour.

FIGURE 15: Model of emergency fuse pin and attachments.
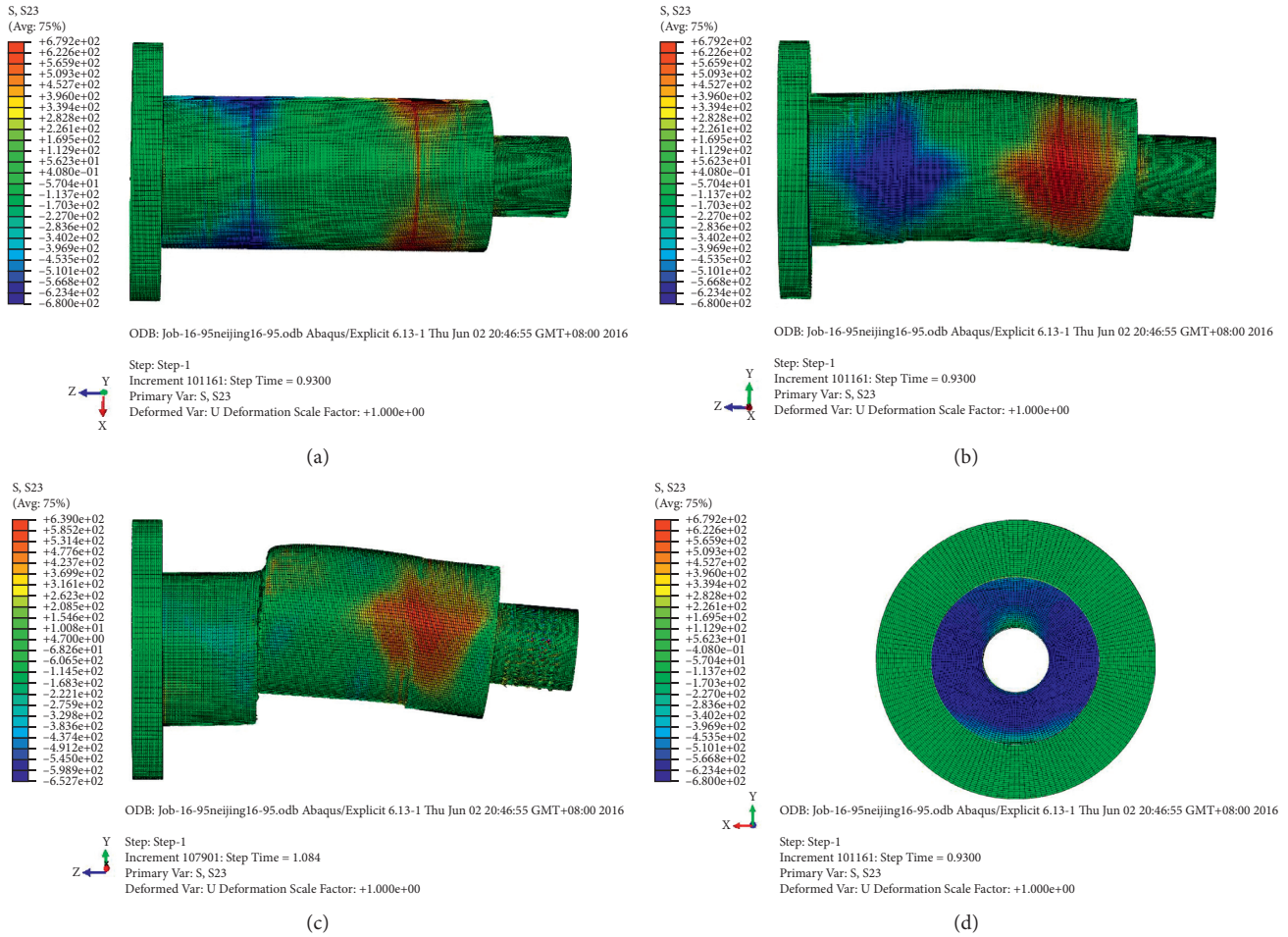
(a)

(b)

(c)

(d)

Figure 16: Fuse pin stress contour at the latest time. (a) Initial moment of load loading. (b) Moment of loading to 70% ultimate load. (c) Separation point. (d) Pin section at the separation point.
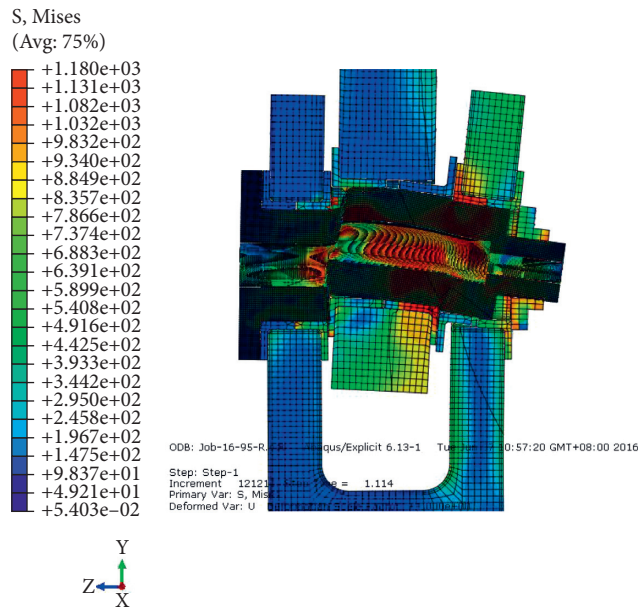

Figure 17: Equivalent stress contour of the fuse pin assembled at the point of failure.
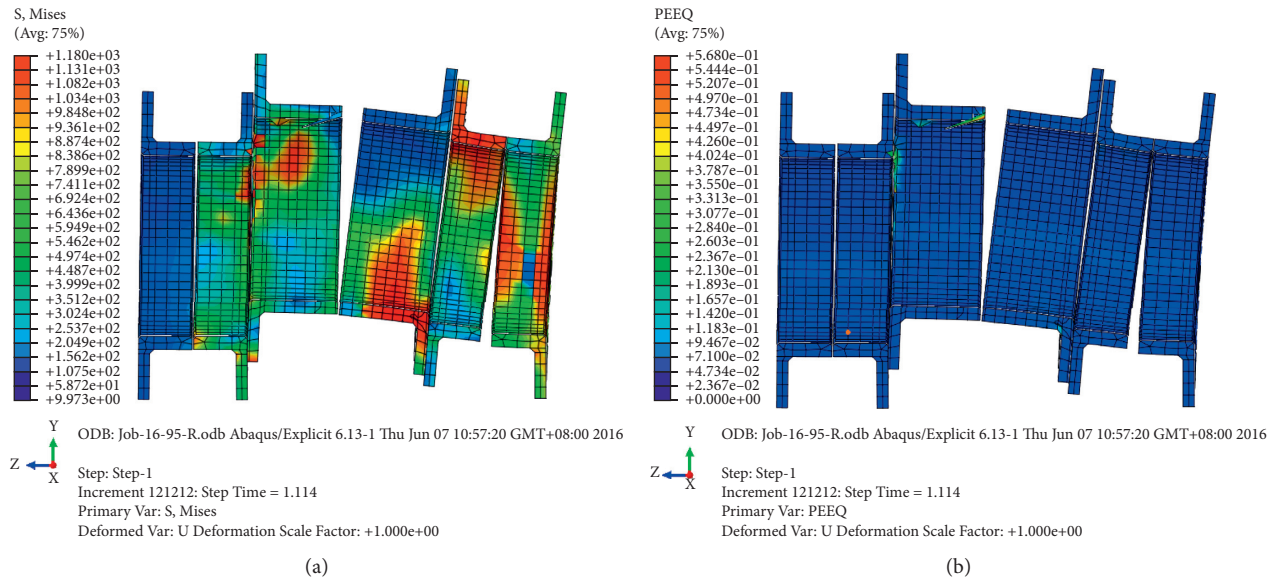
FIGURE 18: Equivalent stress contour of bushing at and after the point of failure. (a) Separation point. (b) After separation.

5.2. Entire Model Simulation. Airworthiness regulations have not provided clear requirements pertaining to emergency landing conditions of aircraft, especially states in which the landing gear is retracted, as well as in terms of pitch angle and cruising and sinking speed. However, a sinking speed of 1.524 m/s is required according to regulation 25.721(b), and the fuel tank structure needed be secure in a controllable landing at the abovementioned sinking speed. The approach speed of a civil aircraft during normal landing is between 66.9 m/s (130 knots) and 82.3 m/s (160 knots), and the controllable landing speed envelope should be a combination of the abovementioned approach speed and sinking speed. For an unplanned emergency landing of the aircraft or a more serious crash landing, the aircraft structure is subjected to larger impacts, and the dynamic responses of the fuse pin and fitting structures are stronger, which makes it more difficult to analyze the separation load.

First, it becomes difficult to determine the exact scenario of emergency separation and calculate the separation loads. Second, it is difficult to determine the structural form of the separation structure and analyze its strength. The process of emergency separation during a wheels-up landing is a highly nonlinear transient thermal coupled dynamics problem. The attitude and impact speed of the aircraft greatly influence the analysis results, and various techniques are required to simulate the separation and crash processes. Failure of the fuse pins and separation of the structure are simulated and analyzed to obtain the time domain loading process and energy conversion and failure mode of the separation structure.

In FE analysis, the interaction between the nacelle, landing gear, and ground is modeled using a general contact algorithm (see Figures 19–21). The general contact algorithm is used to simulate the force and pressure applied during impact. The penalty function of this contact algorithm is the default method for contact problems in ABAQUS/Explicit, which is especially suitable for solving complex contact problems involving different objects and the interiors of the aircraft. The contact analysis must ensure that the components do not penetrate directly without interaction. Three types of contact conditions must be considered in an analysis of the failure of emergency fuse pins: contact between the separation structures and the fitting hole; contact between various regions of the connecting structure after deformation, such as deformation of the ears and other parts after curling; and contact between the nacelle hanging structure and the bottom of the wing panel. For the above three contact situations, a suitable contact pair for simulating contact should be built by combining various types of contact available in ABAQUS/Explicit. For contact between the fuse pins and the fitting structure, the contact position is clear, but it involves subsequent contact calculation of the inner elements after failure of the outer elements of the separation structure. For this reason, the node-to-surface contact setting is used because the connection structure is stiffer than the fuse pins, and its mesh density is higher; the surface of the joint hole is set as the main surface, and the nodes of the fuse pin are set as the slave surface. In cases of the contact caused by deformation and crimping between the connecting structures and the contact between the bottom of the single ear and the nacelle pylon structure, surface contact is adopted. The contact algorithm determines the contact area between the surfaces according to the distance between the contact pairs, checks whether there is mutual penetration, and performs contact calculations. We denote the contact property in ABAQUS/Explicit as hard contact, contact formula as finite slip contact, and tangential contact friction coefficient as 0.15. In this paper, the ABAQUS/Explicit algorithm was used to perform numerical simulation analysis of the upper, middle, and rear separation points. The FE model used in the simulation should be based on the strength and dynamic loads calculation and be validated by the Ground Vibration Test to ensure the accuracy and correctness of the analysis.
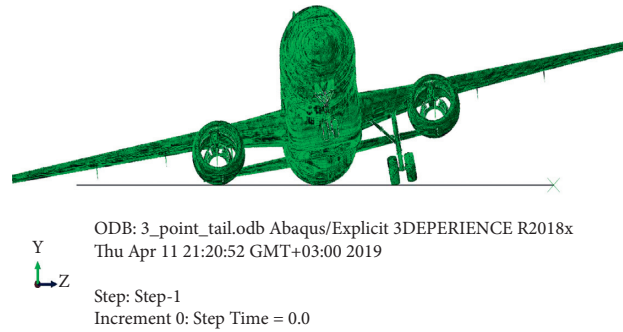
ODB: 3_point_tail.odb Abaqus/Explicit 3DEPERIENCE R2018x
Thu Apr 11 21:20:52 GMT+03:00 2019

Step: Step-1
Increment 0: Step Time = 0.0

FIGURE 19: Model of single wheel-up crash without pitch angle.

70 m/s

Boundary conditions
Wing fixed at the wingbox
to the center wingbox
interface
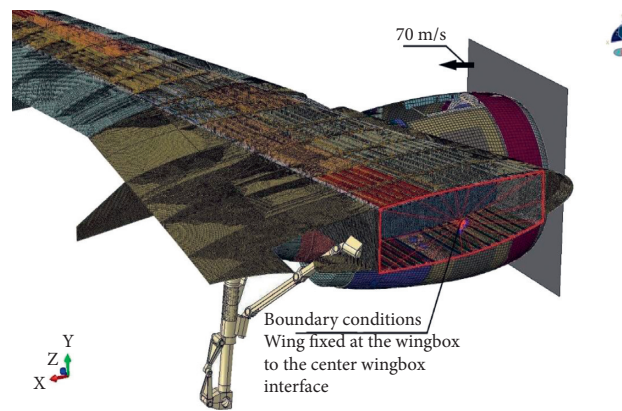
FIGURE 20: One side wing and nacelle model of wheel-up crashing with pitch angle (approaching impact).

Boundary
conditions
Wing fixed at the
wingbox to the
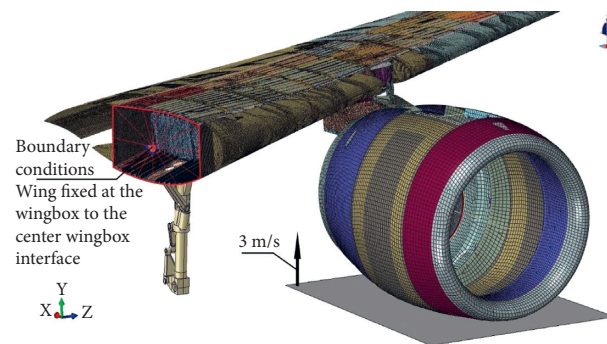center wingbox
interface

3 m/s

FIGURE 21: One side wing and nacelle model of wheel-up crashing with pitch angle (vertical impact).

In the process of wheel-up landing and crashing, the responses of the emergency fuse pins and the interface structure are mainly related to the sinking speed, approach speed, and attitude. Differences between the sinking speed and the approach speed lead to different response of the nacelle and ground impact. This is mainly manifested as different strain rates of the structure, leading to different mechanical response characteristics of the emergency separation structure. In addition, partially or completely retracted landing gear (all three gears retracted, any two gears retracted, and a single gear retracted) affects the impact response of the fuse pins and other interface structures. We simulated an aircraft crash scenario with sinking speeds of 2.43 m/s (8 ft/s), 4.57 m/s (15 ft/s), 7.62 m/s (25 ft/s),

10.67 m/s (35 ft/s), and 15.24 m/s (50 ft/s) and the landing gear retracted, taking into account the impact influence of yaw angle of 20° at the same time. Therefore, in the above analysis, combinations of the yaw situation and the abovementioned sinking speeds were considered to obtain the maximum strain rates and response loads during emergency separation. Then, the dynamic response, loads, strain, and stress at the emergency separation condition are calculated.

In the analysis, because the stiffness of the paved runway was significantly higher than the stiffness of the aircraft structure, the runway was simulated as a rigid surface. In the case of an emergency landing with the wheels retracted, the wing box structure is subjected to reaction force from the
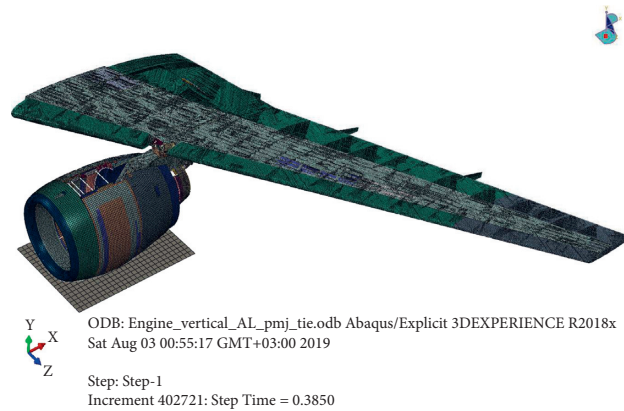
ODB: Engine_vertical_AL_pmj_tie.odb Abaqus/Explicit 3DEXPERIENCE R2018x
Sat Aug 03 00:55:17 GMT+03:00 2019

Step: Step-1
Increment 402721: Step Time = 0.3850

FIGURE 22: Vertical impact model of crash with wheels retracted.

Speed at center the gravity of
the nacelle
V_x=1.545 m/s
V_y=8.309 m/s
V_x=0.054 m/s

ODB: Engine_vertical_AL_pmj_tie.odb Abaqus/Explicit 3DEXPERIENCE R2018x
Wed Jul 31 20:58:00 GMT+03:00 2019

Step: Step-1
Increment 239258: Step Time = 0.2300

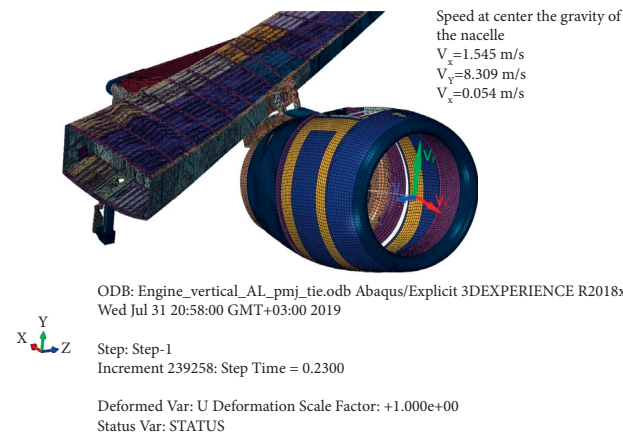Deformed Var: U Deformation Scale Factor: +1.000e+00
Status Var: STATUS

FIGURE 23: Deformation after emergency break—vertical impact.

engine and the aerodynamic force acting on the surface of the wing. It is necessary to simulate aerodynamic loads in the model to investigate the stress state of the wing box and the fuel tank. Under standard atmospheric conditions, at sea level, when the approach speed is 70 m/s and the vertical speed is 3 m/s, the aerodynamic force is equal to the aircraft's maximum landing weight. In this case, the aerodynamic force acting on the entire aircraft in the event of a crash landing with the landing gear retracted is equal to the maximum landing weight of the aircraft. The load is distributed over the entire wing with standard aerodynamic load distribution, and the effect of sweep angle must be considered.

6. Result

Figure 22 shows the FE model of the vertical impact in a single-sided wheel-up landing scenario, including the structural FE models of the wing, nacelle, and pylon. The analysis results indicate that, during a vertical impact, the vertical velocity at the center of gravity of the nacelle reaches 8.3 m/s, and the heading velocity is 1.545 m/s (see Figures 23 and 24). The rear connection point first reaches the peak load value and breaks off. On the time domain curve, the emergency breaking load curve reaches the peak value at 0.255 s and drops rapidly; then, at 0.34 s, the middle connection point reaches the peak load value. After the load peaks, it starts to decrease rapidly to realize unloading. Finally, at 0.4 s, the front connection point reaches the peak load value and declines rapidly thereafter to realize unloading (see Figures 25 and 26). According to a comparison of the analysis results, the emergency separation analysis results of the aircraft in the situation with the wheels retracted provide a more accurate representation of the emergency separation sequence and load value.

FE models of the course of impact in a crash with the wheels retracted are shown in Figure 27. The analysis results show that, during the course impact, the vertical velocity at the center of gravity of the nacelle reaches 5.959 m/s, and the approach velocity is 90 m/s. The middle connection point first reaches the peak load value and separates. On the time domain curve, the emergency breaking load curve peaks at 0.205 s and drops rapidly thereafter; then, at 0.207 s, the front and rear connection points reach their respective peak loads at almost the same time and decline rapidly thereafter (see Figures 28–32). Compared to the vertical crash situation, the transient nature of the course of crash is more obvious. The separation time between the central connection point and the subsequent connection point is only 0.002 s, which
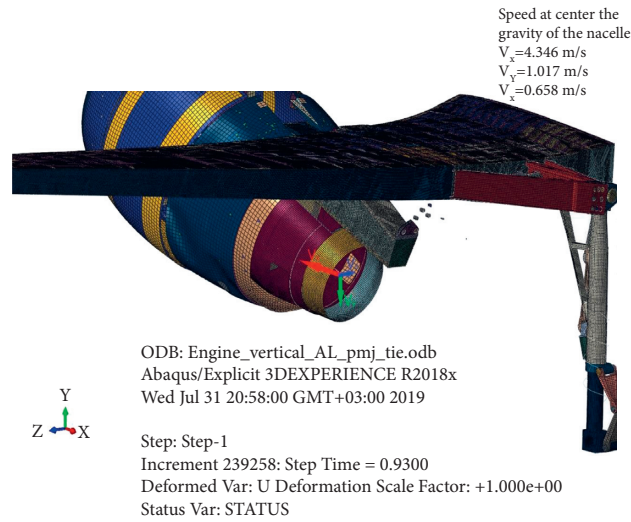
Speed at center the gravity of the nacelle
V_x=4.346 m/s
V_y=1.017 m/s
V_x=0.658 m/s

ODB: Engine_vertical_AL_pmj_tie.odb
Abaqus/Explicit 3DEXPERIENCE R2018x
Wed Jul 31 20:58:00 GMT+03:00 2019

Step: Step-1
Increment 239258: Step Time = 0.9300
Deformed Var: U Deformation Scale Factor: +1.000e+00
Status Var: STATUS

FIGURE 24: Deformation after emergency break—vertical impact.

—— CFT2 on rear down FP
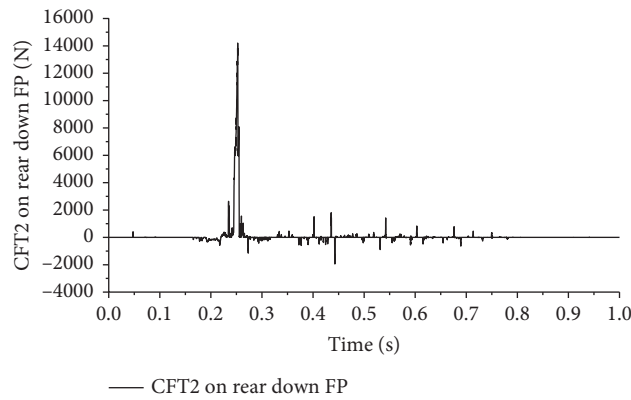
FIGURE 25: Load time domain curve of fuse pins at rear connection point—vertical impact.
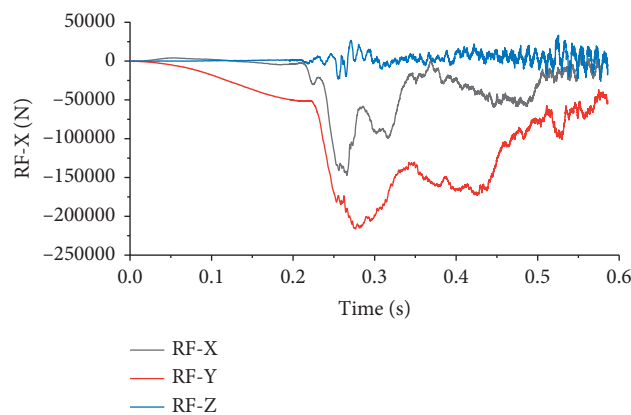

—— RF-X
—— RF-Y
—— RF-Z

FIGURE 26: Emergency disconnection sequence of wheel retraction—vertical impact.

means the two events occur almost simultaneously. According to the morphology of the analysis results, in the case of a vertical impact, the nacelle is separated from the wing structure at an upward turning angle and trajectory.

According to the stress, loads results, and cloud diagrams of the wing structure in Figures 31–33, the central connection point separates firstly (see Figures 29 and 30), and the front and aft point are separated (see Figures 29).
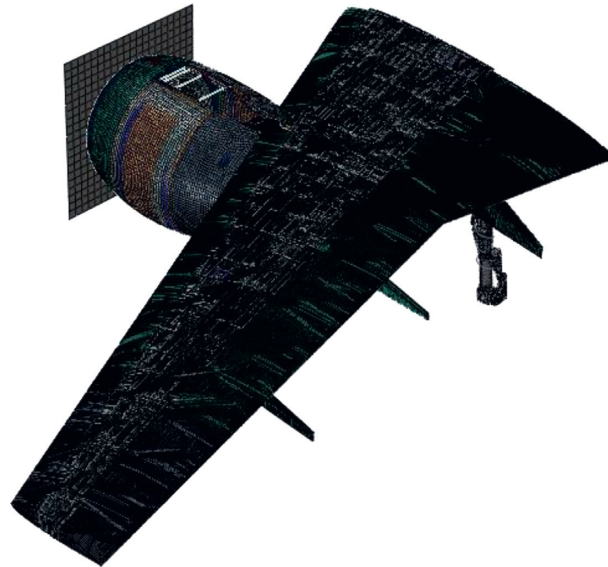
FIGURE 27: Course impact model of crash with wheels retracted.

Speed at center the gravity
of the nacelle
V_x=90.408 m/s
V_y=5.595 m/s
V_x=0.702 m/s

Y
X   Z

ODB: Engine_horizontal_AL_pmj_tie.odb Abaqus/Explicit 3DEXPERIENCE R2018x
Wed Aug 07 14:16:53 GMT+03:00 2019

Step: Step-1
Increment 21352: Step Time = 1.3704E-02

Deformed Var: U Deformation Scale Factor: +1.000e+00
Status Var: STATUS

FIGURE 28: Deformation and velocity of center of gravity after emergency disconnection—course of impact.

VVF
SNEG, (fraction = −1.0)
(Avg: 75%)
+1.404e−02
+1.287e−02
+1.170e−02
+1.053e−02
+9.358e−03
+8.188e−03
+7.019e−03
+5.849e−03
+4.679e−03
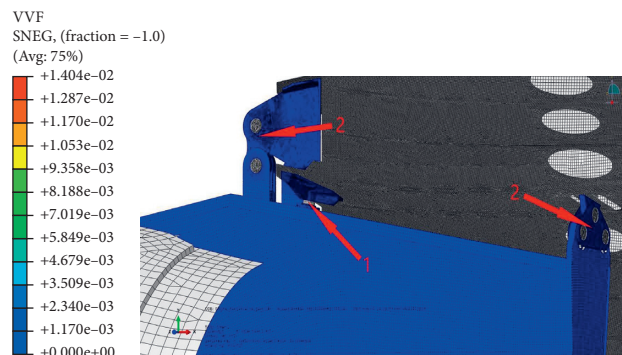+3.509e−03
+2.340e−03
+1.170e−03
+0.000e+00

FIGURE 29: Emergency disconnection sequence of wheel retraction—course of impact.
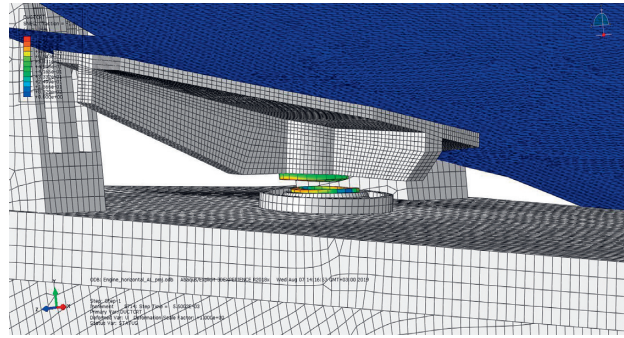
FIGURE 30: Damage to emergency disconnection device at central connection point—course of impact.
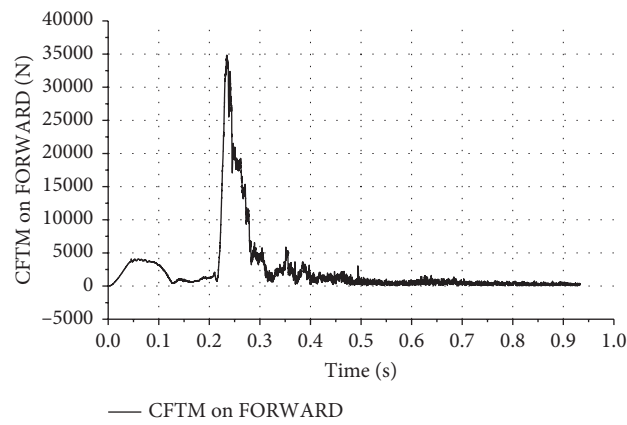

FIGURE 31: Emergency breaking load of front connection point—course of impact.
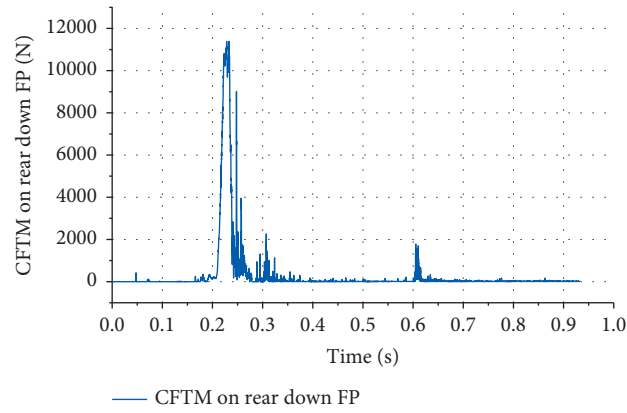

FIGURE 32: Emergency breaking load of rear connection point—course of impact.
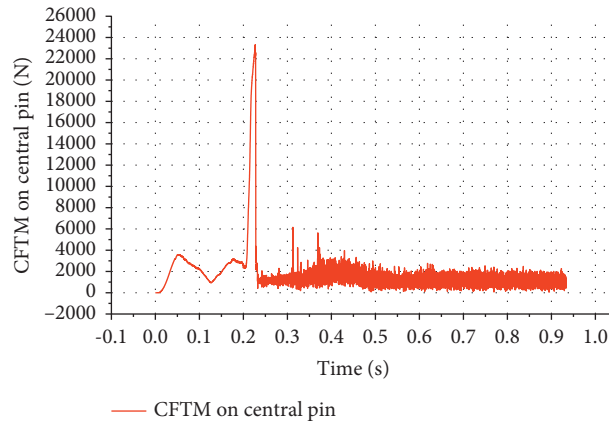
FIGURE 33: Emergency breaking load of intermediate connection point—course of impact.

7. Conclusion

In this study, we numerically simulated the emergency separation process in civilian aircraft by using the nacelle and pylon structure of a typical large airliner. The results indicated that the constitutive parameters and failure strain of metallic materials are directly related to the calculation results of load, stress, and strain during a crash. The strain rate and mesh size were found to be an important parameter to affect the structure damage. Impacts with different sinking velocities during crashing were considered in the simulation and analysis of the nacelle, pylon, and fuse pin structures, as well as that of the entire aircraft. The real elongation and fracture strain were determined experimentally, and the consistency between the analysis data and test data was excellent. The peak load, internal force, and stress level of each structure was lower than the material ultimate strength, indicating that fracture of the fuse pins effectively dissipates the energy generated by the crash and impact process. The main contributions of this paper were to study the scene of the aircraft wheel-up landing separation, and to provide a method of demonstrating compliance with airworthiness regulations based on simulation model and critical structure (such as the fuse pins) tests with the dynamic constitute and damage model.

Data Availability

The data used to support the findings of this study are available from the corresponding author upon request.

Conflicts of Interest

The authors declare that they have no conflicts of interest.

References

[1] Federal Aviation Administration, *Code of Federal Regulation Part 25 Airworthiness Standards (Transports Category Airplanes): FAR-25 (Amendment 25-123)*, Federal Aviation Administration, Washington, DC, USA, 2007.

[2] G. Chen, J. Yang, A. Sergeev et al., "Coupled crash mechanics and biomechanics of aircraft structures and passengers," *Communications in Nonlinear Science and Numerical Simulation*, vol. 101, no. 3, Article ID 105850, 2021.

[3] Z. Jin, D. Li, and J. Xiang, "Crash simulation of fuselage section in the rebound process and the secondary-impact process," *Aircraft engineering and aerospace technology*, vol. 92, no. 8, 2020.

[4] M. Bronstein, E. Feldman, R. Vescovini, and C. Bisagni, "Assessment of dynamic effects on aircraft design loads: the landing impact case," *Progress in Aerospace Sciences*, vol. 78, pp. 131–139, 2015.

[5] H. Wang, D. Wu, F. Wang, P. Liu, and X. Tu, "A new method for determining horizontal impact load based on rotational speed of aircraft wheel in landing gear drop test," *MATEC Web of Conferences*, vol. 114, p. 03004, 2017.

[6] S. Li, Q. Duan, D. Cao, Y. Zhong, and H. Hu, "Calculation of landing crash load of civil aircraft wheel retracted," *Chinese Journal of Applied Mechanics*, vol. 35, no. 5, pp. 1008–1014+1183, 2018.

[7] W. Zhang, *Simulation Analysis and Research on the Fallability of the Fuselage Section of Civil Aircraft*, Shanghai Jiao tong University, Shanghai, China, 2011.

[8] X. Liu, "Civil aircraft fuselage section and cabin facilities crash test and structural fallability evaluation," *Journal of Aeronautics*, vol. 34, no. 9, pp. 2130–2140, 2013.

[9] M. A. Iqbal, S. Rai, M. R. Sadique, and P. Bhargava, "Numerical simulation of aircraft crash on nuclear containment structure," *Nuclear Engineering and Design*, vol. 243, pp. 321–335, 2012.

[10] M. Mahesh and M. Subrata, "Finite element analysis of time-dependent inelastic deformation in the presence of transient thermal stresses," *International Journal for Numerical Methods in Engineering*, pp. 909–921, 1981.

[11] Z.-C. Lin and W.-S. Yang, "Rolling process analysis of aluminum strip by a coupled thermo-elastic-plastic model," *International Journal of Machine Tools and Manufacture*, vol. 35, no. 4, pp. 619–635, 1995.

[12] C. Bertrand-Corsini, C. David, and A. Bern, "A three-dimensional thermomechanical analysis of steady flows in hot forming processes," *Application to Hot Flat Rolling and Hot Shape Rolling*, vol. 20, no. 4, 1988.

[13] N. L. Mat, A. R. S. Beyon, and H. L. Yiu, "Thermomechanical modelling of aluminium alloy rolling," *Journal of Materials Processing Technology*, vol. 45, no. 1-4, pp. 631–636, 1994.

[14] L. Malcher, F. M. César de Sá, and J. M. A. C. de Sá, "An assessment of isotropic constitutive models for ductile

fracture under high and low stress triaxiality," *International Journal of Plasticity*, vol. 30-31, pp. 81–115, 2012.

[15] J. M. C. Rodrigues and P. A. F. Martins, "Coupled thermo-mechanical analysis of metal-forming processes through a combined finite element-boundary element approach," *International Journal for Numerical Methods in Engineering*, vol. 42, no. 4, pp. 631–645, 2015.

[16] A. Bragov, A. Konstantinov, A. Lomunov, I. Sergeichev, and B. Fedulov, "Experimental and numerical analysis of high strain rate response of ti-6al-4v titanium alloy," *Toxicon Official Journal of the International Society on Toxinology*, vol. 2, p. 1465, 2009.

[17] H. Wu, L. Yu, and W. Jiang, "A coupling FEM/BEM method with linear continuous elements for acoustic-structural interaction problems," *Applied Acoustics*, vol. 150, pp. 44–54, 2019.

[18] H. Dyja and P. Korczak, "The thermal-mechanical and microstructural model for the FEM simulation of hot plate rolling," *Journal of Materials Processing Technology*, vol. 92-93, pp. 463–467, 1999.

[19] G. Zhou, L. Hua, D. Qian, D. Shi, and H. Li, "Effects of axial rolls motions on radial-axial rolling process for large-scale alloy steel ring with 3D coupled thermo-mechanical FEA," *International Journal of Mechanical Sciences*, vol. 59, no. 1, pp. 1–7, 2012.

[20] M. Tanaka and K. Miyazawa, "Study ON the shear strength OF double shear test OF bolt joint with steel plate: p," *Journal of Structural and Construction Engineering (Transactions of AIJ)*, vol. 70, no. 589, pp. 143–148, 2005.

[21] Z. Hashin and A. Rotem, "A fatigue failure criterion for fiber reinforced materials," *Journal of Composite Materials*, vol. 7, no. 4, pp. 448–464, 1973.

[22] Z. Hashin, "Failure criteria for unidirectional fiber composites," *Journal of Applied Mechanics*, vol. 47, no. 2, pp. 329–334, 1980.